Theoretical and Experimental *SAR* Distributions for Interstitial Dipole Antenna Arrays Used in Hyperthermia

KENNETH M. JONES, MEMBER, IEEE, JOYCE A. MECHLING, MEMBER, IEEE,
JOHN W. STROHBEHN, SENIOR MEMBER, IEEE,
AND B. STUART TREMBLY, MEMBER, IEEE

Abstract—**Theoretical predictions and experimental measurements of power deposition in muscle tissue phantoms from arrays of microwave dipole antennas used for hyperthermia cancer therapy are compared. The antennas are linear coaxial dipoles, constructed from coaxial cable approximately 1 mm in diameter, which are inserted into small nylon catheters implanted in the tumor volume. The antennas have a tip section consisting of an expanded extension of the inner conductor, and a second section consisting of the outer conductor and extending from the tip section back to the insertion point into the tissue or phantom. In this work these two sections have equal length; i.e. the antennas are symmetrical dipoles. The specific absorption rate (*SAR*, W/kg) patterns for a 2 cm square array of four 915 MHz antennas are presented for both resonant and nonresonant dipoles. Arrays of dipoles with lengths much shorter than the resonant half-wavelength have a far more reactive input impedance and a much smaller absolute *SAR* magnitude in the array center than is seen for arrays of resonant dipoles, and the maximum *SAR* shifts from the array center to the antenna surfaces. The absolute length of the volume heated by the small-diameter antennas with the longer half-wavelength was longer than that for the larger diameter antennas. *SAR* distributions for 4 cm square arrays of eight and nine antennas fed with equal amplitude and phase are also compared. It is found that much of the array volume has a power deposition less than 25 percent of the maximum *SAR* and that the distribution is nonuniform for both the eight- and nine-antenna configurations.**

I. Introduction

TYPICAL TUMORS encountered in the clinic can range from 2 to 10 cm in diameter, and tumor sites vary from being on the skin surface to deep within the brain or pelvis. The primary objective of any hyperthermia system is to raise the temperature in the tumor volume to 43°–55°C while the surrounding normal tissue remains below 44°C. Several noninvasive hyperthermia systems, e.g., microwave and ultrasound external applicators, inductive coils, and RF annular phased arrays, are being investigated clinically as possible treatment modalities [1]–[3]. While systems for treating superficial tumors often may meet these specifications, all present systems have major problems for tumors more than a few centimeters from the skin surface [4]–[6]. Furthermore, the monitoring of tissue temperature presents a problem, since no practical methods presently exist to measure temperatures accurately and noninvasively a few centimeters beneath the skin.

Interstitial microwave antenna array hyperthermia (IMAAH) systems are being investigated by several groups as a feasible treatment modality for tumors of various sizes and at different sites [7]–[13]. Although these systems are invasive and hence will not be applicable for many sites, where feasible and with appropriate antenna design, they show the potential to customize the power deposition properties to the specifications of the tumor size and location. Both theory and experiment have been used to verify that the single 915 MHz insulated antenna used at the Dartmouth-Hitchcock Medical Center will shift the maximum longitudinal power distribution to coincide with the electrical junction between the two sections regardless of insertion depth [14], [15]. This feature enables the physician to insert a single antenna so the maximum power deposition is within the tumor volume regardless of tumor location. The clinician can also tailor the power distribution to cover a tumor of arbitrary transverse extent by implanting a sufficient number of antennas in an array.

Another motivation for developing interstitial hyperthermia techniques is that they can be used as an adjuvant to brachytherapy (radioactive seeds implanted in catheters). When the interstitial system has been designed to operate with the catheter spacing dictated by brachytherapy considerations, the two modalities are complementary and introduce little additional risk to the patient [9], [16]–[18]. Furthermore, in some situations thermometry probes can be inserted in the brachytherapy catheters to allow measurement of temperatures in both tumor and surrounding normal tissues.

Studies of power deposition properties for single insulated dipole antennas used in the IMAAH treatment sys-

Manuscript received September 21, 1987; revised December 29, 1988. This work was supported in part by the National Science Foundation under Grants ECS-8307032 and ECS-83522580 and by the National Institute of Health (CA 42604)

K. M. Jones is with the LTX Corporation, Westwood, MA.

J. A. Mechling, B. S. Trembly, and J. W. Strohbehn are with the Thayer School of Engineering, Dartmouth College, Hanover, NH 03755.

IEEE Log Number 8928325.

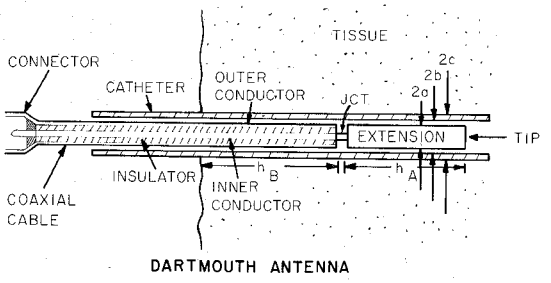

Fig. 1. Schematic of the insulated antenna design showing section A with length h_A and section B with length h_B. Typically h_A is fixed while h_B is a function of the depth of the treatment site or depth the antenna is inserted in phantom. The diameter of the coaxial cable is $2a$, the inner catheter diameter is $2b$, and the outer catheter diameter is $2c$ (from Strohbehn and Mechling, 1986).

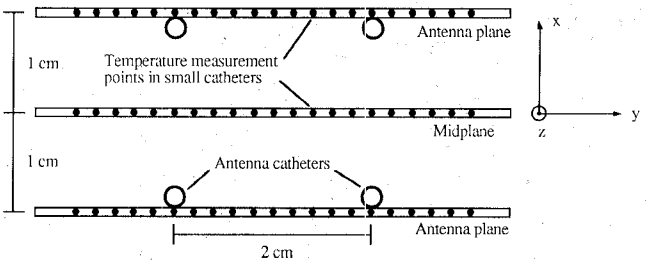

Fig. 2. Schematic of catheter placement in phantom box for longitudinal array measurements. The antenna catheters go into the page, and the thermometer catheters used for measuring *SAR* are shown. The midplane is parallel to the antennas and extends through the array center. An antenna plane contains two antennas on the side of the array and is parallel to the midplane. The dot in the antenna catheter indicates points where *SAR* measurements are made and are separated by 2 mm.

tem at the Dartmouth-Hitchcock Medical Center have been reported previously [14]. Three design parameters were investigated: (1) resonant and nonresonant dipole antenna lengths; (2) antenna catheter thickness; and (3) nonsymmetrical antenna lengths. In this paper, both theory and experiment are applied to an investigation of specific absorption rate (*SAR*, W/kg) distributions for interstitial dipole antenna arrays. Theoretical and experimental *SAR* distributions for a 2 cm square array of four 915 MHz symmetrical antennas are presented for both resonant and nonresonant dipoles and for different catheter thicknesses. Lastly, *SAR* distributions for 4 cm square arrays, composed of either eight or nine antennas, are compared to reveal the detrimental effect of destructive phase interference when arrays of more than four antennas are driven in phase.

The *SAR* is the average power absorbed per unit mass of tissue and is given by

$$SAR\left(\frac{\mathrm{W}}{\mathrm{kg}}\right) = \frac{1}{2}\frac{\sigma}{\rho}|\boldsymbol{E}|^2 \qquad (1)$$

where σ (mho/m) is the conductivity of the tissue, ρ (kg/m^3) is the density of the tissue, and $|\boldsymbol{E}|$ (V/m) is the magnitude of the electric field.

All cases (both theoretical and experimental) are for 915 MHz antennas driven coherently in phantom with the electrical properties of skeletal muscle [19]. The theoretical *SAR* curves were calculated by computer programs based on theoretical results previously reported [20]. The experimental procedure is described below.

The basic antenna design is shown in Fig. 1, and the theory of operation has been described elsewhere [16], [20], [21]. Briefly, the antenna consists of three transmission lines to which normal transmission line theory applies. The energy from the generator creates a voltage at the junction, i.e., the gap between the end of the outer conductor and the extension of the inner conductor. This voltage establishes currents which travel along the outside of section A from the junction to the tip and along the outside of section B from the junction to the tissue–air interface. These currents induce the electromagnetic wave that is propagated into the tissue. The driving frequency, section lengths h_A and h_B, the various radii defined in Fig. 1, and the electrical properties of the catheter and tissue determine the antenna input impedance and the electrical field distribution. It is assumed in the theoretical development that the antennas are independent and that mutual coupling effects are negligible.

II. Experimental Techniques

The *SAR* measurement procedure has been described in detail elsewhere [8], [22], [23], and is based on the rate of temperature change caused by the radiated power from the microwave antennas. Prior to phantom construction, antenna catheters (1.8 mm ID, 2.2 mm OD) were strung horizontally in a cast acrylic container (14 cm×13 cm×14 cm) to form a square array with 2 cm spacing between adjacent catheters. Smaller catheters, to be used as pathways from the temperature probes, were strung perpendicularly to the antenna catheters with 1 cm spacing between adjacent catheters, thereby filling the array volume. Fig. 2 shows one plane of temperature catheters. These planes of catheters were spaced at 1 cm intervals along the antennas; the number of planes was determined by the length of the antenna. Steel rods were inserted in all catheters to hold them firmly in place while the phantom material was poured around them and allowed to solidify for at least 12 h.

Prior to an *SAR* experiment, the antennas were inserted in the large catheters to form an array of the desired size. Up to 12 fiber-optic thermometry probes were inserted in the smaller catheters with their sensors aligned at one edge of the desired measurement range. During an experiment, temperatures in the tissue-equivalent phantom material were recorded over a period of 60 s after power to the antennas was turned on. All the probes were then moved 2 mm by a stepper motor, controlled by the computer, to the next measurement nodes. The phantom was then allowed to cool to equilibrium before the process was repeated. The rate of temperature rise was estimated [15], [23], and the

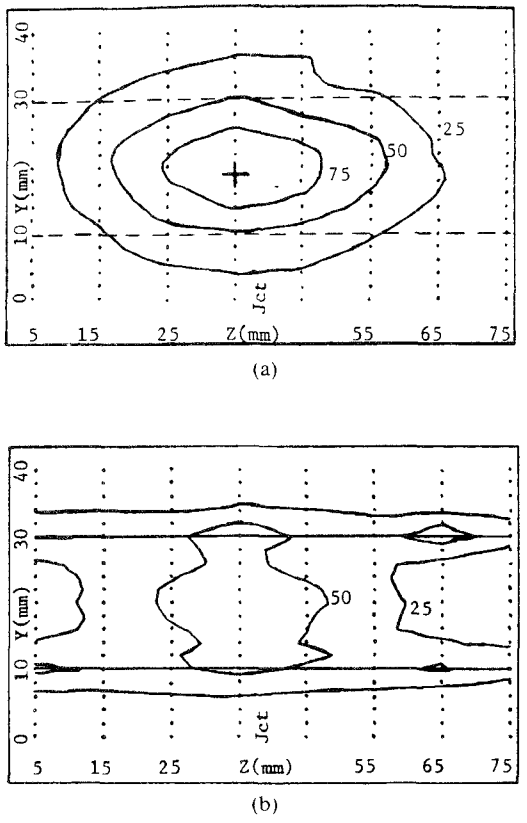

Fig. 3. Experimental *SAR* distributions for a 2 cm square array of four 0.9 mm OD resonant half-wavelength dipole antennas in 1.2 mm ID, 2.2 mm OD catheters ($h_A = h_B = 3.9$ cm): (a) midplane; (b) antenna plane. Maximum absolute *SAR* (denoted by "+") was 752 W/kg. The vertical rows of dots indicate the points where the *SAR* was measured. The dashed horizontal lines in (a) indicate the plane where the antennas are located. The solid horizontal lines in (b) indicate the location of the antennas.

SAR calculated by

$$SAR\left(\frac{\mathrm{W}}{\mathrm{kg}}\right) = c\left.\frac{\partial T}{\partial t}\right|_{t=10\,\mathrm{s}} \tag{2}$$

where T is temperature (°C), t is time (s), and c is the specific heat of the tissue (W·s/kg·°C). Chou *et al.* [24] have measured the specific heat of the muscle phantom at 915 MHz to be 3601 W·s/kg·°C. It should be noted that iso-*SAR* plots measured with our *SAR* measurement system are repeatable with a variation of less than ±5 percent [15]. If identical experiments are performed and then averaged, the variation is decreased.

In this paper, experimental *SAR* results for 2 cm square arrays are presented as measured by the procedure described above. For most cases, the results from two measurement planes are used to characterize the performance of the antennas in an array. The midplane is defined as a plane through the array center and parallel to the antenna axes (Fig. 2) and shows the longitudinal *SAR* distribution between the antennas. The antenna plane is parallel to the midplane but includes two antennas forming the side of an array (Fig. 2). Fig. 3(a) and (b) shows iso-*SAR* plots for the midplane and antenna plane, respectively. The results shown in Fig. 3(a) are for a single experiment. The plot shown in Fig. 3(b), on the other hand, is the average of two experiments, one for each of the antenna planes shown in Fig. 2. The iso-*SAR* contours shown are 25 percent, 50 percent, and 75 percent of the maximum *SAR* that was measured in the array. The contours are constructed by simple linear interpolation between measurement points. The "+" symbol indicates the location of the maximum absolute *SAR* for each antenna and catheter configuration investigated. Note that in Fig. 3, this symbol is marked only in the midplane, where the global *SAR* maximum occurs. The antenna locations are represented by horizontal dashed lines in the midplane plot and by horizontal solid lines in the antenna plane plot. The label "Jct" marks the axial location of the antenna junction.

Experiments for four-antenna arrays (Figs. 3–6, 8–11) were performed at an input power of 65 W as measured at the generator. The eight-antenna experiment shown in Fig. 12(a) was run at an input power of 120 W. The feed cable from the generator to the antennas has a constant loss of approximately 30 percent of the power measured at the generator [15]. The maximum *SAR* values given in the figures are for these conditions.

III. Results

The purpose of the investigation of resonant versus nonresonant arrays was to observe any differences between the two cases in both the transverse and longitudinal power distributions. A thick-walled catheter was used for this experiment to ensure that the antennas were lying concentrically within their catheters; it allows no air gap around the antenna. If this precaution had not been taken, measurement error could have resulted due to changes in input impedance and nonuniform radiation around the antenna circumference [15], [23].

Fig. 3 shows the experimental performance of a four-antenna array of 0.9 mm OD resonant dipole antennas in 1.2 mm ID, 2.2 mm OD catheters. It indicates that the region of greatest power deposition was around the center of the array, where by the center of the array we mean the point in the midplane that is in the junction plane and halfway between the two dashed lines. Furthermore, the area enclosed by the 50 percent contour in the antenna plane is approximately 2 cm square. As a measure of longitudinal heating performance, we define the ratio between the length of the 50 percent iso-*SAR* contour in the midplane, L_{50}, and the dipole antenna length, L_d ($L_d = h_A + h_B$). This ratio was 0.50 for the resonant dipole of length 7.8 cm shown in Fig. 3(a); i.e., L_{50} was approximately 3.9 cm. It has been shown experimentally that L_{50} also was approximately 3.9 cm for a single antenna with the same design as those used in Fig. 3 [14]. The maximum absolute *SAR* in the array was measured in the midplane with a magnitude of 752 W/kg, as calculated from (2).

Fig. 4 shows the corresponding theoretical iso-*SAR* plots. The locations of the antennas are represented in the antenna plane by solid lines. Note from Fig. 4(a) that the measure of longitudinal power deposition, L_{50}/L_d, was essentially identical to the experimental case, i.e., 0.50. The

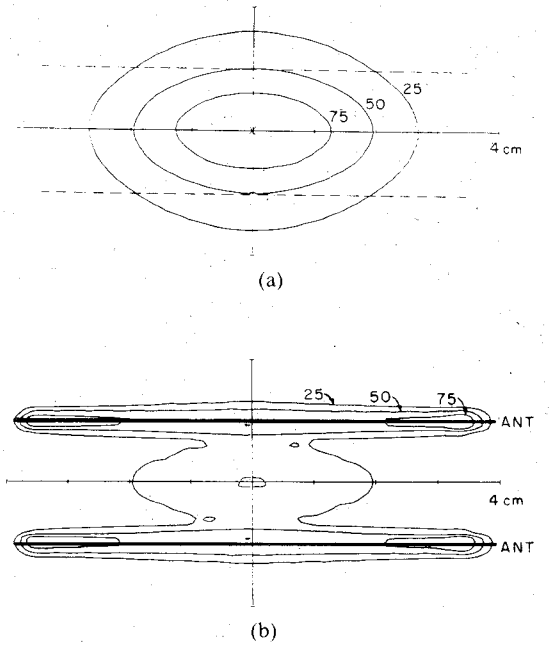

Fig. 4. Theoretical *SAR* distributions for a 2 cm square array of four 0.9 mm OD resonant half-wavelength dipole antennas in 1.2 mm ID, 2.2 mm OD catheters ($h_A = h_B = 3.9$ cm): (a) midplane; (b) antenna plane. Maximum absolute *SAR* (denoted by "+") was 1.1 W/kg (1 V at junction).

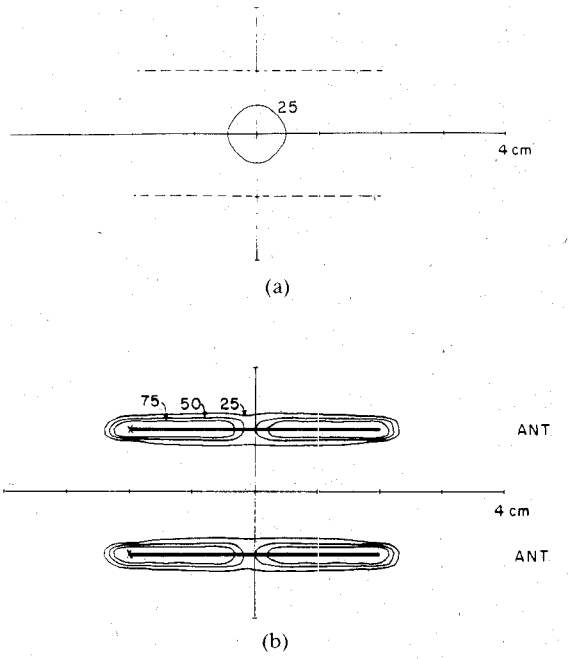

Fig. 6. Theoretical *SAR* distributions for a 2 cm square array of four 0.9 mm OD nonresonant dipole antennas in 1.2 mm ID, 2.2 mm OD catheters ($h_A = h_B = 2.0$ cm): (a) midplane; (b) antenna plane. Maximum absolute *SAR* (denoted by "+") was 0.2 W/kg (1 V at junction).

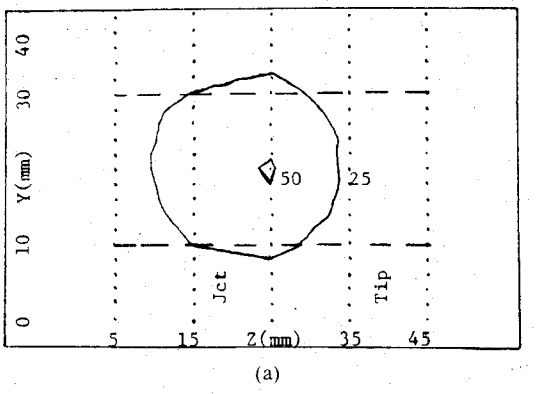

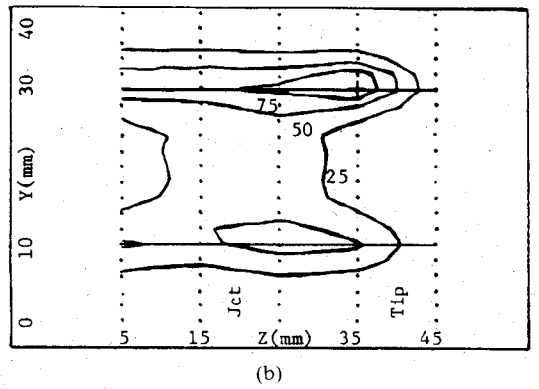

Fig. 5. Experimental *SAR* distributions for a 2 cm square array of four 0.9 mm OD nonresonant dipole antennas in 1.2 mm ID, 2.2 mm OD catheters ($h_A = h_B = 2.0$ cm): (a) midplane; (b) antenna plane. Maximum absolute *SAR* (denoted by "+") was 749 W/kg.

antenna plane in Fig. 4(b) was quite similar to the experiment, although the 50 percent contour was smaller. (Note that all *SAR* contours are relative to the maximum *SAR* measured or calculated in the array.) As expected, the maximum power deposition was at the array center, and the power deposition was symmetric about the junction plane. The absolute magnitude was 1.1 W/kg, as calculated from (1). Note that theoretical *SAR* values are based on the antennas with an emf of 1 V at the junction rather than an input power level. Therefore, only comparisons of relative *SAR* were made.

The experimental performance of an array of 0.9 mm OD nonresonant dipole antennas in thick catheters is shown in Fig. 5. Section lengths h_A and h_B were 2 cm each, i.e., approximately half of the resonant quarter-wavelength of 3.9 cm. The label "Tip" indicates the end of the antenna deepest within the phantom. The magnitude of the maximum absolute *SAR* was 749 W/kg, nearly equal to the value of the resonant dipoles in Fig. 3. However, the maximum *SAR* was in the midplane for the resonant case but in the antenna plane for the nonresonant case. The magnitude of the maximum absolute *SAR* in the midplane was only 393 W/kg, half of that measured for the resonant dipole case, and L_{50}/L_d was essentially zero.

The corresponding theoretical results are shown in Fig. 6. The midplane in Fig. 6(a) does not contain a 50 percent contour as was seen in the experimental results. In the antenna plane, it was predicted that much of the array volume had a power deposition less than 25 percent of the maximum *SAR*. The maximum predicted power levels were at the antennas, at the insertion point of each antenna. Note that the calculated maximum absolute *SAR*

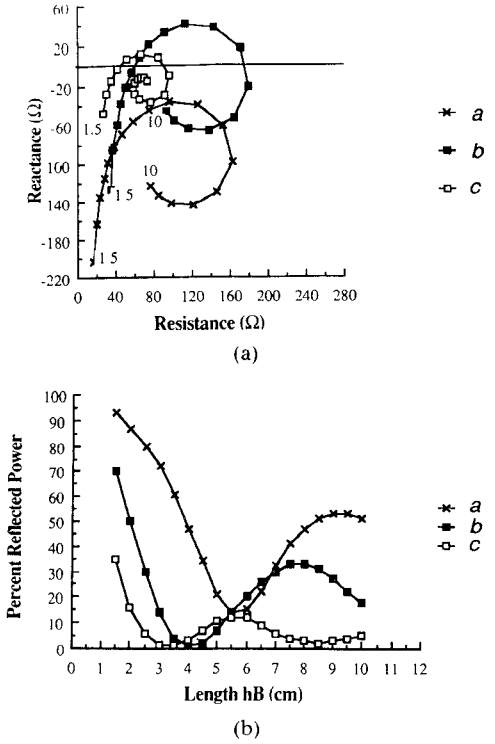

Fig. 7. (a) Theoretical antenna input impedance and (b) percent reflected power as a function of length h_B for three antenna configurations. *a*: 0.9 mm OD antenna in 1.2 mm ID, 2.2 mm OD catheter, $h_A = 2.0$ cm; *b*: 0.9 mm OD antenna in 1.2 mm ID, 2.2 mm OD catheter, $h_A = 3.9$ cm (resonant); *c*: 1.6 mm OD antenna in 1.8 mm ID, 2.2 mm OD catheter, $h_A = 2.7$ cm (resonant).

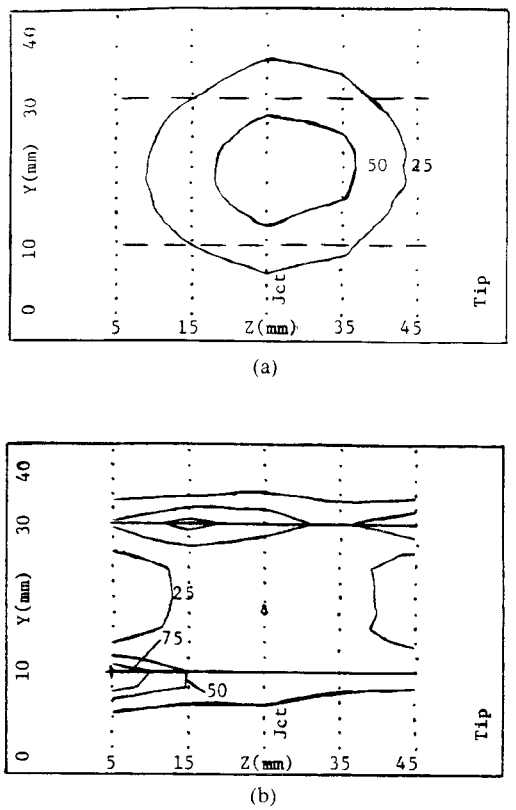

Fig. 8. Experimental *SAR* distributions for a 2 cm square array four 1.6 mm OD resonant half-wavelength dipole antennas in 1.8 mm ID, 2.2 mm OD catheters ($h_A = h_B = 2.7$ cm): (a) midplane; (b) antenna plane. Maximum absolute *SAR* (denoted by "+" was 1112 W/kg.

was only 0.2 W/kg, much smaller than that of 1.1 W/kg for the theoretical resonant dipoles in Fig. 4. These results also are explained by considering the antenna input impedances of both the resonant and nonresonant antennas.

Fig. 7 shows graphs of theoretical antenna input impedance and percentage of reflected power as a function of length h_B for three of the antenna configurations presented in this paper. It has been shown that these theoretical impedance data qualitatively represent experimental impedance data [14], [15]. The calculated impedance and percent reflected power (Fig. 7) for the resonant dipole antenna array ($h_A = h_B = 3.9$ cm) shown in Figs. 3 and 4 were $(56 - i6)$ Ω and 1 percent, respectively. These values indicate that the impedance match between the antenna and the 50 Ω feedline was very good and hence that nearly all of the power was radiated from the array. Furthermore, since this antenna design has been shown to couple well to the medium [14], the maximum *SAR* was at the array center for both theory and experiment. However, for the nonresonant dipole antenna array ($h_A = h_B = 2.0$ cm) shown in Figs. 5 and 6, the impedance was $(20 - i163)$ Ω and the reflected power was 87 percent, indicating a large impedance mismatch. Thus in theory only 13 percent of the power was radiated from the array. This explains why the absolute *SAR* magnitudes at the array centers were small when compared to those for the resonant array. Furthermore, it has been shown that this short antenna design does not couple well to the medium and the radial *SAR* distribution is poor [14]. This explains why the maximum absolute *SAR* values shifted from the array centers, as seen for the resonant arrays of Figs. 3 and 4, to the antenna surfaces, as seen for the short, nonresonant arrays of Figs. 5 and 6.

It should be noted that all theoretical *SAR* plots shown were symmetric for dipole antennas because the defined antenna parameters for section *A* were identical to the parameters in section *B* [20]. Experimental *SAR* results were not necessarily symmetric, probably due in part to differences in the termination impedances of sections *A* and *B* and in part to the fact that no two antennas are identical. This issue has been discussed in more detail in [14].

Fig. 8 shows the experimental *SAR* distribution for 1.6 mm OD (large) resonant dipole ($h_A = h_B = 2.7$ cm) antennas in 1.8 mm ID, 2.2 mm OD (thin) catheters. The corresponding theoretical results are shown in Fig. 9. This case was investigated to observe any differences in the longitudinal *SAR* patterns when compared to the results in Figs. 3 and 4 for 0.9 mm OD (small) resonant dipole antennas ($h_A = h_B = 3.9$ cm) in 1.2 mm ID, 2.2 mm OD (thick) catheters. This experiment was performed for single antennas and it was found that no differences in the *SAR* distributions could be detected [14]. A comparison of the theoretical results in Figs. 4 and 9 indicates that the small antennas in the thick catheters ($h_A = h_B = 3.9$ cm) were

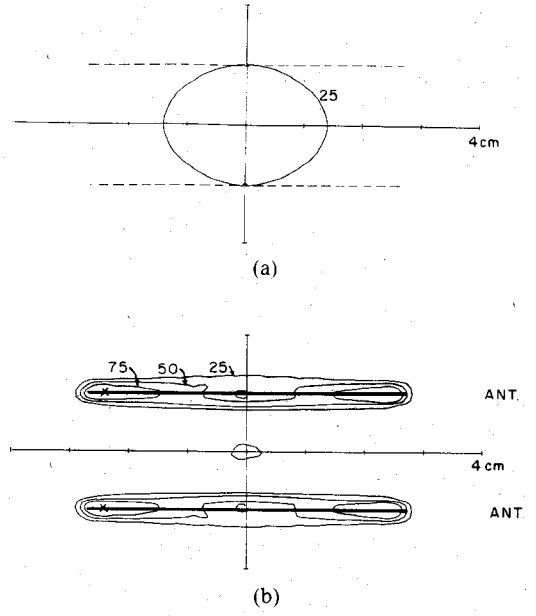

Fig. 9. Theoretical *SAR* distributions for a 2 cm square array of four 1.6 mm OD resonant half-wavelength dipole antennas in 1.8 mm ID, 2.2 mm OD catheters ($h_A = h_B = 2.7$ cm): (a) midplane; (b) antenna plane. Maximum absolute *SAR* (denoted by "+") was 3.7 W/kg (1 V at junction).

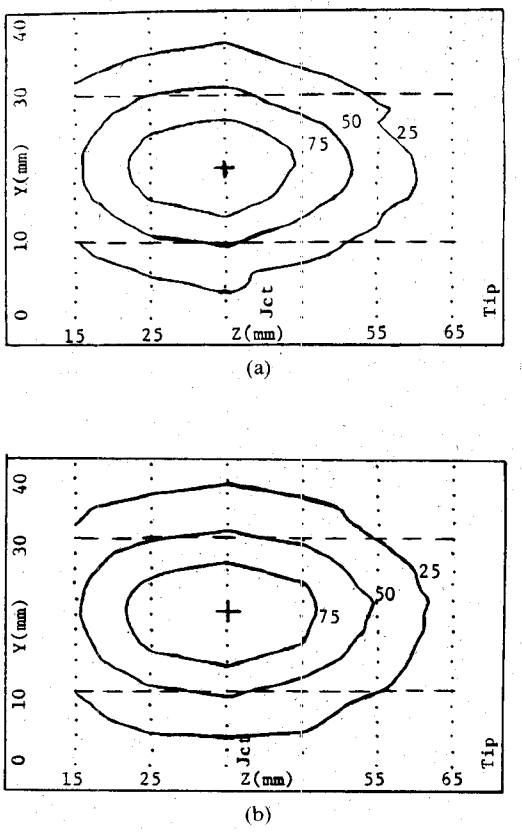

Fig. 10. Two experimental *SAR* distributions in the midplanes for 2 cm square arrays of four nonresonant dipole antennas ($h_A = h_B = 3.5$ cm): (a) 0.9 mm OD antenna in 1.2 mm ID, 2.2 mm, OD catheter; (b) 1.6 mm OD antenna in 1.8 mm ID, 2.2 mm OD catheter. Maximum absolute SAR is denoted by "+."

able to deposit power more uniformly throughout the array volume than the larger antennas in the thin catheters ($h_A = h_B = 2.7$ cm). The absolute length of the volume heated by the small-diameter antennas with the longer total length ($L_{50} = 3.9$ cm) was greater than that for the larger diameter antennas ($L_{50} = 0.0$ cm). Clinically, this indicates that a larger tumor can be heated with the longer antennas. Both cases produced 75 percent contours at the antenna tips and insertion points.

The experimental results (Fig. 8(a)) demonstrate that the midplane of the large antenna in the thin catheter ($h_A = h_B = 2.7$ cm) did not contain a 75 percent contour while the midplane for the small antenna in the thick catheter ($h_A = h_B = 3.9$ cm, Fig. 3(a)) contained the maximum value of *SAR*. Therefore, experiment indicates that the power distribution for the large antenna in the thin catheter was somewhat more uniform in the longitudinal direction through the array center.

The increase in longitudinal *SAR* uniformity demonstrated for the large antennas in the thin catheters (Fig. 8(a)) resulted in a trade-off, since the maximum *SAR* values were at the antenna surfaces rather than in the array center. This result was seen in both theory (Fig. 9(b)) and experiment (Fig. 8(b)). As in the case of the 4.0 cm dipole (Fig. 5), the shift of the maximum *SAR* from the array center to the antennas was an indication that short dipoles do not radiate as well into the medium. Hence, the transverse *SAR* distribution is poor for short dipoles, and the fields are not strong enough to produce a maximum *SAR* at the array center.

It has been shown theoretically and experimentally for single antennas that the antenna and catheter dimensions, especially section lengths h_A and h_B, independently affect both the input impedance and the *SAR* distribution [14], [20], [21]. Fig. 7 shows that the theoretical antenna input impedance for the large antenna in the thin catheter ($h_A = h_B = 2.7$ cm, Fig. 9) was $(37 - i8)\ \Omega$ and the reflected power was 3 percent. While these impedance values are similar to those given for the small antenna in the thick catheter ($h_A = h_B = 3.9$ cm, Fig. 4), the experimental results indicated a difference in the *SAR* distributions. In order to discern whether this difference was due to catheter thickness or antenna length, a comparison was made between cases with the two different catheter thicknesses and equal antenna lengths. Theoretical and experimental studies were performed for an array of large-diameter antennas in thin-walled catheters and an array of small-diameter antennas in thick-walled catheters in which both antennas were nonresonant dipoles of total length equal to 7.0 cm.

Experimental and theoretical results for the midplanes of both cases are shown in Figs. 10 and 11, respectively. Experiment indicates that the *SAR* distributions were nearly identical for the two configurations. The antenna planes also demonstrate nearly identical distributions [15]. Experimentally, the L_{50}/L_d ratio was 0.5 for the small antenna in the thick catheter (Fig. 10(a)) and 0.57 for the large antenna in the thin catheter (Fig. 10(b)). Theoretically, these ratios were 0.49 and 0.33 for the small and large antennas, respectively. Therefore, the longitudinal

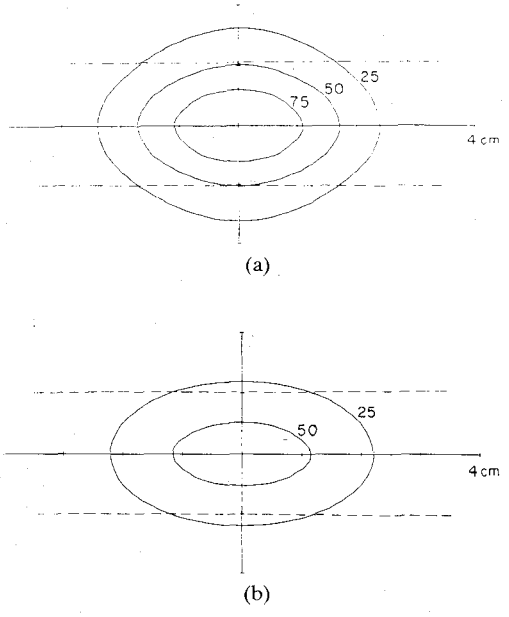

Fig. 11. Two theoretical *SAR* distributions in the midplanes for 2 cm square arrays of four nonresonant dipole antennas ($h_A = h_B = 3.5$ cm): (a) 0.9 mm OD antenna in 1.2 mm ID, 2.2 mm OD catheter; (b) 1.6 mm OD antenna in 1.8 mm ID, 2.2 mm OD catheter.

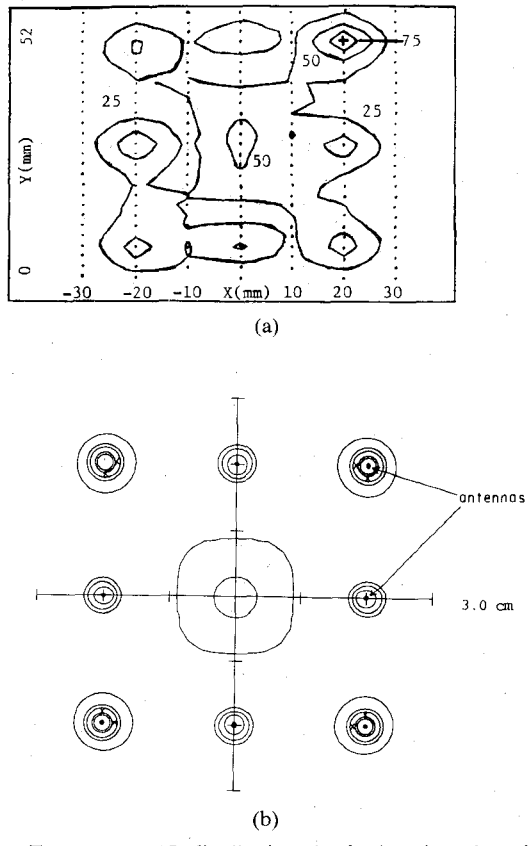

Fig. 12. Transverse *SAR* distributions in the junction plane for eight 1.6 mm OD nonresonant dipole antennas in 1.8 mm ID, 2.2 mm OD catheters in a 4 cm square array ($h_A = h_B = 3.5$ cm): (a) experiment; (b) theory. Maximum absolute *SAR* in the junction plane is denoted by "+."

SAR distribution was longer for the case of the small antenna in the thick catheter; yet, in practice, this difference is small. In both cases, experimentally the maximum *SAR* was at the center of the antenna array while theoretically the maximum was at the antennas.

The experimental and theoretical transverse, junction plane *SAR* distributions for an eight-antenna array are shown in Fig. 12. Note that this plane is transverse to the antennas and orthogonal to the planes displayed in previous figures. The array was 4 cm square with the antennas evenly spaced along the sides at 2 cm intervals. The antennas were 1.6 mm OD dipoles with nonresonant section lengths equal to 3.5 cm. The theory agrees reasonably well with the experimental results. The patterns show large variation, and most of the power deposition within the array was below 25 percent of the maximum *SAR*. As an alternative to this case, the theoretical *SAR* was calculated for an array of the same dimensions with a ninth antenna at the array center. Fig. 13(a) shows a plane cutting diagonally through the array and parallel to the antennas for the eight-antenna case. Note that Fig. 13 shows a plane perpendicular to Fig. 12(b) and along a diagonal line going from the upper left corner to the lower right corner. As shown in Fig. 12, the power distribution is not uniform, and it is below 25 percent of the maximum *SAR* over much of the array volume. A diagonal cut through the nine-antenna array is shown in Fig. 13(b). Although the *SAR* distribution is perhaps more uniform, the array center has less than 25 percent of the maximum *SAR*. Further study is needed to evaluate how effective these *SAR* patterns will be in creating desirable temperature distributions.

IV. Conclusions

It is well known in conventional antenna theory that for many purposes it is desirable to operate linear dipole antennas with each section equal to a quarter-wavelength. For the purposes of this study, where the power deposition in the near field is of interest, the experimental and theoretical results confirm the importance of using antennas operating at close to their resonant length for good performance. At or close to resonance the antenna impedance was close to 50 Ω and the reflected power was quite low. For antennas whose total length was equal to a quarter-wavelength the antenna impedance was large and reactive, and most of the power was reflected. While it is known that the reflected power can be decreased substantially by the use of stub tuners or other matching networks, we have shown previously that double stub tuners can cause unpredictable *SAR* distributions by introducing unknown phase shifts among antennas [8], [25]. In addition, for the resonant antennas the *SAR* patterns were more desirable in that the *SAR* pattern had a maximum in the center of a 2 cm square array, while this local maximum disappeared for antennas half as long.

When the outer diameter of the catheter is held constant but the radius of the antenna is varied, there is a large change in the resonant length. We held the outer catheter

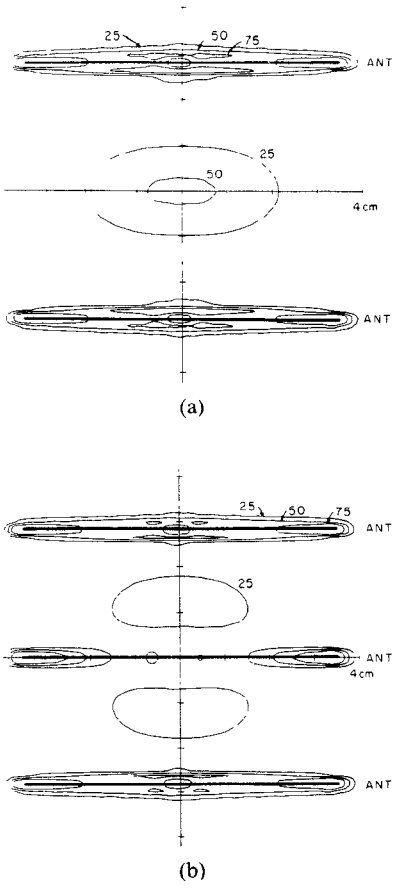

Fig. 13. Theoretical longitudinal *SAR* distributions along a diagonal plane for 1.6 mm OD nonresonant dipole antennas in 1.8 mm ID, 2.2 mm OD catheters in a 4 cm square array ($h_A = h_B = 3.5$ cm): (a) eight antennas; (b) nine antennas.

diameter at 2.2 mm and performed tests with antenna diameters of 0.9 and 1.6 mm, resulting in resonant half-wavelengths of 7.8 and 5.4 cm, respectively. The ratio L_{50}/L_d was about the same for both cases, and hence the longer antenna had a longer *SAR* pattern. However, the thinner antennas resulted in much higher power deposition in the center of the array, while the shorter antenna had the maximum *SAR* at an antenna instead of in the center. On the other hand, for 7.0 cm length antennas the *SAR* patterns for the thin and thick antennas were very similar. All of the *SAR* measurements were compared with theoretical predictions and in most cases showed good agreement. These results give us confidence in the accuracy and usefulness of the theoretical formulas in [20] and [21].

The results for four-antenna arrays show *SAR* patterns that are reasonably uniform and of interest for hyperthermia treatments. Both the theoretical and experimental results for eight and nine antennas implanted in a 4 cm square show large variations in the *SAR* pattern. Clearly, these more complex arrays result in regions of constructive and destructive interference which produce these large variations. More work needs to be done both theoretically and experimentally to understand the importance of these complex *SAR* patterns. If these patterns are not satisfactory, then more complex systems will need to be devised, which might include varying phase [26].

Single antennas with the tip section a quarter-wavelength and the h_B section much longer have been investigated and the results are encouraging [14]. It has been shown that the region of maximum *SAR* shifts longitudinally to coincide with the junction, regardless of insertion depth. When h_B is approximately a half-wavelength, the longitudinal power distribution increases significantly. When h_B is much longer than a half-wavelength, the input impedance approaches a constant value, and the *SAR* pattern becomes constant and similar to that of a half-wavelength antenna, and symmetric about the junction. Further studies are needed to see if these single-antenna effects are present for arrays. Preliminary evidence indicates that the effect of insertion depth on arrays may be more complex than for the single-antenna case [27], [28].

In summary we conclude that these dipole antennas have a number of desirable properties for hyperthermia treatments, but it is important that users understand their properties in order to apply them correctly. First, it is desirable that the antennas be operated so that the tip section is equal or close to a quarter-wavelength, where the wavelength is that of the antenna in a composite medium [20]. Second, small antennas in thicker catheters have a longer wavelength and also generally perform better. Third, the impedance of resonant antennas is usually close to 50 Ω, and the reflected power is small. Fourth, the *SAR* pattern of four antennas on the corners of a 2 cm square array has a maximum in the center and agrees with theory.

There are certain drawbacks to these antennas. First, the *SAR* patterns for the arrays show that not much energy is deposited near the tips. Second, the overall length of the *SAR* pattern is not as long as desirable for some tumors, and it is difficult to change this longitudinal length. Third, when more than four antennas are used, the *SAR* pattern exhibits great complexity. We have not found the lack of tip heating to be a major problem in the clinic, although there are times when it becomes an issue. The longitudinal length can be changed over a small range, provided that the user understands the basic physics of the antennas. The *SAR* patterns of large numbers of antennas need to be studied in more depth to understand the importance of the problem and possible solutions. Finally, as our work has shown, it is important to understand how arrays of these antennas behave and not to rely completely on the results of single-antenna measurements, as they can be misleading.

ACKNOWLEDGMENT

The authors would like to thank T. P. Ryan for his help with the equipment and advice on measurement protocols during this work.

REFERENCES

[1] J. W. Hand and J. R. James, Ed., *Handbook of Techniques for Clinical Hyperthermia*. Chichester, England Research Studies Press, 1986.

[2] F. K. Storm, Ed., *Hyperthermia in Cancer Therapy* Boston: Hall Medical Publishers, 1983.

[3] J. W. Strohbehn, "Evaluation of hyperthermia equipment," in *Hyperthermia in Cancer Treatment*, L. J. Anghileri and J. Robert, Eds. Boca Raton, FL: CRC Press, 1986, pp. 179–198.
[4] K. D. Paulsen, J. W. Strohbehn, and D. R. Lynch, "Comparative theoretical performance for two types of regional hyperthermia systems," *Int. J. Radiat. Oncol. Biol. Phys.*, vol. 11, pp. 1659–1671, 1985.
[5] M. D. Sapozink, F. A. Gibbs, Jr., K. S. Gates, and J. R. Stewart, "Regional hyperthermia in the treatment of clinically advanced, deep seated malignancy: Results of a pilot study employing an annular array applicator," *Int. J. Radiat. Oncol. Biol. Phys.*, vol. 10, pp. 775–786, 1984.
[6] J. R. Oleson, R. S. Heusinkveld, and M. R. Manning, "Hyperthermia by magnetic induction: II. Clinical experience with concentric electrodes," *Int. J. Radiat. Oncol. Biol. Phys.*, vol. 9, pp. 549–556, 1983.
[7] J. W. Strohbehn, B. S. Trembly, and E. B. Douple, "Blood flow effects on the temperature distributions from an invasive microwave antenna array used in cancer therapy," *IEEE Trans. Biomed. Eng.*, vol. BME-29, pp. 649–661, 1982.
[8] T. Z. Wong, J. W. Strohbehn, K. M. Jones, J. A. Mechling, and B. S. Trembly, "*SAR* patterns from an interstitial microwave antenna array hyperthermia system," *IEEE Trans. Microwave Theory Tech.*, vol. MTT-34, pp. 560–567, 1986.
[9] C. T. Coughlin *et al.*, "Intra-operative interstitial microwave-induced hyperthermia and brachytherapy," *Int. J. Radiat. Oncol. Biol. Phys.*, vol. 11, pp. 1673–1678, 1985.
[10] D. W. Roberts, C. T. Coughlin, T. Z. Wong, E. B. Douple, and J. W. Strohbehn, "Interstitial hyperthermia and iridium brachytherapy in the treatment of malignant glioma: A phase 1 clinical trial," *J. Neurosurgery*, vol. 64, pp. 581–587, 1986.
[11] B. Emami and C. A. Perez, "Interstitial thermoradiotherapy—An overview," *ECHO* vol. 1, pp. 35–40, 1985.
[12] P. F. Turner, "Interstitial equal-phased arrays for EM hyperthermia," *IEEE Trans. Microwave Theory Tech.*, vol. MTT-34, pp. 572–578, 1986.
[13] G. M. Samaras, "Intracranial microwave hyperthermia: Heat induction and temperature control," *IEEE Trans. Biomed. Eng.*, vol. BME-31, pp. 63–69, 1984.
[14] K. M. Jones, J. A. Mechling, B. S. Trembly, and J. W. Strohbehn, "Theoretical and experimental SAR distributions for an interstitial microwave antenna for hyperthermia," *IEEE Trans. Biomed. Eng.*, vol. MTT-35, pp. 851–857, 1988.
[15] K. M. Jones, "Evaluation and improvement of an interstitial microwave antenna array hyperthermia system", M.E. thesis, Thayer School of Engineering, Dartmouth College, Hanover, NH, May 1987.
[16] J. W. Strohbehn, and J. A. Mechling, "Interstitial techniques of clinical hyperthermia," in *Handbook of Techniques for Clinical Hyperthermia*, J. W. Hand and J. R. James, Eds. England: Research Studies Press, 1986.
[17] J. M. Cosset *et al.*, "Combined interstitial hyperthermia and brachytherapy: Institute Gustave Roussy technique and preliminary results," *Int. J. Radiat. Oncol. Biol. Phys.*, vol. 10, pp. 307–312, 1984.
[18] M. R. Manning, *et al.*, "Clinical hyperthermia: Results of a phase I trial employing hyperthermia along or in combination with external beam or interstitial radiotherapy," *Cancer*, vol. 49, pp. 205–216, 1982.
[19] A. W. Guy, "Analyses of electromagnetic fields induced in biological tissues by thermographic studies on equivalent phantom models," *IEEE Trans. Microwave Theory Tech.*, vol. MTT-19, pp. 205–214, 1971.
[20] R. W. P. King, B. S. Trembly, and J. W. Strohbehn, "The electromagnetic field of an insulated antenna in a conducting or dielectric medium," *IEEE Trans. Microwave Theory Tech.*, vol. MTT-31, pp. 574–583, 1983.
[21] B. S. Trembly, "The effects of driving frequency and antenna length on power deposition within a microwave antenna array used for hyperthermia," *IEEE Trans. Biomed. Eng.*, vol. BME-32, pp. 152–157, 1985.
[22] T. Z. Wong, J. W. Strohbehn, and E. B. Douple, "Automated measurement of power deposition patterns from interstitial microwave antennas used in hyperthermia," in *Proc. 11th Northeast Bioeng. Conf.*, 1985, pp. 58–61.
[23] K. M. Jones, T. P. Ryan, and J. W. Strohbehn, "An investigation of three potential errors that can occur in common experimental SAR measurements," in *Proc. 13th Northeast Bioeng. Conf.*, 1987, pp. 386–389.
[24] C. K. Chou, G. W. Chen, A. W. Guy, and K. H. Luk, "Formulas for preparing phantom muscle tissue at various radiofrequencies," *Bioelectromagnetics*, vol. 5, pp. 435–441, 1984.
[25] K. M. Jones, T. Z. Wong, J. A. Mechling, B. S. Trembly, and J. W. Strohbehn, "SAR patterns from an interstitial microwave antenna array hyperthermia system," in *Proc. 12th Northeast Bioeng. Conf.*, 1986, pp. 209–212.
[26] B. S. Trembly *et al.*, "Control of the *SAR* pattern within an interstitial microwave array through variation of antenna driving phase," *IEEE Trans. Microwave Theory Tech.*, vol. MTT-34, pp. 568–571, 1986.
[27] D. L. Denman *et al.*, "The distribution of power and heat produced by interstitial microwave antenna arrays: I. Comparative phantom and canine studies," *Int. J. Radiat. Oncol. Biol. Phys.*, vol. 14, pp. 127–137, 1988.
[28] D. L. Denman, *et al.*, "The distribution of power and heat produced by interstitial microwave antenna arrays: II. The role of antenna spacing and insertion depth," *Int. J. Radiat. Oncol. Biol. Phys.*, vol. 14, pp. 537–545, 1988.

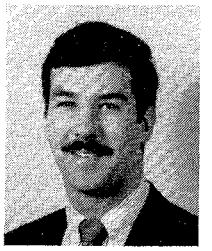

Kenneth M. Jones (S'84–M'87) received the A.B. degree from Dartmouth College, Hanover, NH, in 1985 and the B.E. and M.E. degrees from the Thayer School of Engineering, Dartmouth College, in 1987.

He is currently employed as a Hardware/Software Design Engineer at LTX Corporation in Westwood, MA.

Joyce A. Mechling (S'85–M'87) received the B.S. degree in botany in 1978 and the M.S.E. degree in environmental and water resources engineering in 1982 from the University of Michigan, Ann Arbor.

Between 1978 and 1982 she was employed as a Research Assistant for the Department of Civil Engineering and the Great Lakes Research Division at the University of Michigan and NOAA's Great Lakes Environmental Research Laboratory in Ann Arbor, MI. She is presently a Ph.D. candidate at the Thayer School of Engineering at Dartmouth College, Hanover, NH. Her research interest is in the development of computer models to be used in planning the hyperthermic treatment of cancer.

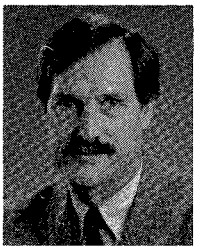

John W. Strohbehn (S'57–M'64–SM'81) received the B.S., M.S., and Ph.D. degrees in electrical engineering from Stanford University, Stanford, CA, in 1958, 1959, and 1964, respectively.

He joined the faculty at the Thayer School of Engineering, Dartmouth College, Hanover, NH, in 1963, where he currently holds the position of Professor of Engineering. His research efforts have been in the fields of radiophysics, including microwave and optical propagation through the atmosphere, and in biomedical engineering, in-

cluding image processing tomography and the use of heat in the cure and control of cancer.

Dr. Strohbehn is a Fellow of the Optical Society of America and a member of the American Association for the Advancement of Science and URSI Commission II. He was a National Academy Exchange Scientist to the Soviet Union in 1964. He served as an Associate Editor of the IEEE TRANSACTIONS OF ANTENNAS AND PROPAGATION from 1969 to 1971 and as an Associate Editor of the IEEE TRANSACTIONS ON BIOMEDICAL ENGINEERING from 1981 to 1987. Dr. Strohbehn was a Visiting Research Scientist at the Stanford University Medical School in 1981–1982. He was Acting Provost of Dartmouth College from 1987 to 1989, and presently is Provost.

B. Stuart Trembly (M'83) received the B.S. degree from Yale University, New Haven, CT, in 1975, and the Ph.D. degree from Dartmouth College, Hanover, NH, in 1982.

He joined the faculty at the Thayer School of Engineering at Dartmouth College in 1982, where he is an Associate Professor. His research interest is the application of electrical engineering to biomedical problems.

Dr. Trembly was the recipient of a Presidential Young Investigator Award in 1984.